Meteoritics & Planetary Science 38, Nr 7, 1005–1021 (2003)
Abstract available online at http://meteoritics.org

The Morávka meteorite fall: 3. Meteoroid initial size, history, structure, and composition

J. BOROVIČKA,[1*] H. W. WEBER,[2] T. JOPEK,[3] P. JAKEŠ,[4] Z. RANDA,[5] P. G. BROWN,[6] D. O. REVELLE,[7] P. KALENDA,[8] L. SCHULTZ,[2] J. KUCERA,[5] J. HALODA,[4] P. TÝCOVÁ,[4] J. FRÝDA,[9] and F. BRANDSTÄTTER[10]

[1]Astronomical Institute of the Academy of Sciences, 25165 Ondrejov, The Czech Republic
[2]Max-Plank-Institut für Chemie, Joh. J.-Becher-Weg 27, D–55128 Mainz, Germany
[3]Astronomical Observatory of A.Mickiewicz University, Sloneczna 36, 60286 Poznan, Poland
[4]Institute of Geochemistry, Mineralogy and Mineral Resources, Faculty of Science, Charles University, Albertov 6, 12843 Prague 2, The Czech Republic
[5]Nuclear Physics Institute, Academy of Sciences, 25068 Rez near Prague, The Czech Republic
[6]Department of Physics and Astronomy, University of Western Ontario, London, Ontario N6A 3K7, Canada
[7]Los Alamos National Laboratory, P. O. Box 1663, MS J557, Los Alamos, New Mexico 87545, USA
[8]CoalExp, Kosmonautu 2, 70030 Ostrava 3, The Czech Republic
[9]Czech Geological Survey, Geologická 6, 15200 Prague 5, The Czech Republic
[10]Department of Mineralogy and Petrography, Museum of Natural History, Burgring 7, A–1010 Vienna, Austria
[*]Corresponding author. E-mail: borovic@asu.cas.cz

(Received 06 September 2002; revision accepted 25 June 2003)

Abstract–The properties and history of the parent meteoroid of the Morávka H5–6 ordinary chondrites have been studied by a combination of various methods. The pre-atmospheric mass of the meteoroid was computed from fireball radiation, infrasound, seismic signal, and the content of noble gases in the meteorites. All methods gave consistent results. The best estimate of the pre-atmospheric mass is 1500 ± 500 kg. The fireball integral bolometric luminous efficiency was 9%, and the acoustic efficiency was 0.14%. The meteoroid cosmic ray exposure age was determined to be $(6.7 \pm 1.0) \times 10^6$ yr. The meteorite shows a clear deficit of helium, both ^{3}He and ^{4}He. This deficit can be explained by solar heating. Numerical backward integration of the meteoroid orbit (determined in a previous paper from video records of the fireball) shows that the perihelion distance was probably lower than 0.5 AU and possibly as low as 0.1 AU 5 Ma ago. The collision which excavated Morávka probably occurred while the parent body was on a near-Earth orbit, as opposed to being confined entirely to the main asteroid belt. An overview of meteorite macroscopic properties, petrology, mineralogy, and chemical composition is given. The meteorites show all mineralogical features of H chondrites. The shock level is S2. Minor deviations from other H chondrites in abundances of trace elements La, Ce, Cs, and Rb were found. The ablation crust is enriched with siderophile elements.

INTRODUCTION

The fall of the Morávka H5–6 ordinary chondrites in the Czech Republic on May 6, 2000 became one of the best documented meteorite falls in history. The corresponding fireball was videotaped by 3 casual witnesses and sonic booms were recorded by 16 seismic stations in the Czech Republic and Poland and by 1 infrasonic station in Germany. Satellites in Earth orbit detected part of the fireball light curve. Six meteorites with a total mass of 1.4 kg have been recovered up to May 2003. Borovička et al. (2003) gave an overview of the events associated with the fall, determined the fireball trajectory and orbit from the video records, and presented the satellite observed light curve. Brown et al. (2003) described and interpreted in detail the infrasonic and seismic data.

In this paper, we concentrate on the pre-atmospheric properties and history of the meteoroid. Various methods, which are usually used separately, are employed to determine the meteoroid initial mass. Cosmic ray exposure age and gas retention age are then determined from the concentration of noble gases in the meteorites, and a helium deficit is revealed.

These data are combined with the numerical backward integration of the meteoroid orbit in the solar system. Finally, the overview of the meteorite macroscopic properties, petrology, mineralogy, and chemical composition is given. In the last paper of the series (Borovička and Kalenda 2003), the atmospheric fragmentation of the meteoroid is studied.

METEOROID INITIAL MASS

The estimation of the meteoroid initial mass is an important part of the description of the meteorite fall. Since we know the initial velocity quite well (22.5 ± 0.3 km/s), the determination of mass is equivalent to the determination of kinetic energy brought to the atmosphere. We also know the bulk density of the meteorites (3.59 ± 0.06 g/cm^3), so we can express the mass in terms of the meteoroid size, provided that the meteorites are representative samples of the meteoroid and assuming a spherical shape of the meteoroid. The initial mass can be estimated from fireball radiation, from the infrasound, and from the analysis of noble gases and cosmogenic nuclides in the meteorites. We will also try to use the seismic data. Each of these methods include extensive modeling and/or the introduction of coefficients that are not well-known nor entirely reliable. We will first discuss the methods separately and then combine their results.

Estimate from Fireball Radiation

In this estimate, we make use of the knowledge of the radiated energy as measured by satellites and recomputed for the whole electromagnetic spectrum (2.5×10^{10} J). The satellite registered only the brightest part of the fireball (see Borovička et al. 2003). Nevertheless, we estimate that the total energy radiated during the 10 sec of fireball duration was not higher by more than 50%. Therefore, the value 3.5×10^{10} J will be used.

The percentage of the meteoroid kinetic energy consumed for radiation is expressed by the coefficient called luminous efficiency. For our purposes, the integral luminous efficiency—defined as the ratio of total radiated energy over the entire spectrum to the difference of kinetic energy at the beginning and at the end of the fireball (see Ceplecha et al. 1998)—is useful. Unfortunately, the integral luminous efficiency is not well known, and it seems to vary widely from fireball to fireball. Empirical values for 33 fireballs derived by Ceplecha et al. (1998; Table 8) are from 0.2% up to 10%. These values were computed for the panchromatic band and are to be increased by a factor of ~3 to convert them to the radiation in whole spectrum. Most of the fireballs listed by Ceplecha et al. (1998) are smaller bodies. Only the fireball PN 40503 was comparable to Morávka. Its panchromatic luminous efficiency was 4.2%, corresponding to a total efficiency of about 12%.

The luminous efficiency of the satellite-detected fall of the St-Robert H5 chondrite was estimated to be ~10% (Brown et al. 1996). Another fireball comparable to Morávka is the well-observed Benešov fireball with a total radiated energy of 5×10^{10} J and initial velocity of 21.2 km/s (Borovička and Spurný 1996). The initial mass was found to be 3000–4000 kg by Borovička et al. (1998) and 4100 kg by ReVelle and Ceplecha (2002). This gives the luminous efficiency of 5.5–7.5%. Nemtchinov et al. (1997) computed integral luminous efficiencies theoretically. For the Morávka composition, velocity, and radiated energy, the theoretical values are 10%.

Combining the information above, we give the conservative estimate of 10% ± 5% for the integral luminous efficiency of Morávka. This transforms to the meteoroid initial energy of 3.5×10^{11} J (with limits $2.5–7 \times 10^{11}$ J) and a mass of 1400 kg (1000–2800 kg).

Estimate from the Infrasound

The infrasonic signal from the Morávka fireball recorded at station IS26 in Freyung, Germany is described in detail in Brown et al. (2003). Three distinct signal arrivals, called trains #1 to #3, were detected. They were interpreted as an anomalous stratospheric, a normal stratospheric, and a thermospheric return, respectively.

From the infrasonic data, we can derive approximate source energies incorporating a variety of assumptions. These techniques and their limitations are discussed in detail in ReVelle and Whitaker (1999) as well as ReVelle (1976).

The most commonly applied technique for infrasonic energy measurements is the period at maximum amplitude approach (ReVelle 1997), which is based on an empirical relation between the observed period at maximum signal amplitude (P) for stratospheric returns and known yields (E in kilotons of TNT = 4.185×10^{12} J) for US nuclear tests (ReVelle 1980):

$$\log\frac{E}{2} = 3.34\log(P) - 2.58 \quad (1)$$

This relation has been applied to a large number of energetic bolide events (ReVelle 1997) and found to be in reasonable agreement with other independent energy estimates for the same events. For our infrasonic signal, the typical stratospheric return (train #2) has a period of 4.1 ± 0.8 sec. These measurements are from the zero-crossings for each of the 4 channels and are produced using an average and standard deviation from all 4 channels. This corresponds to an energy given by Equation 1, E = 0.59 ± 0.28 kT = (2.5 ± 1.2) $\times 10^{12}$ J.

Another method for estimating energy release is the use of acoustic efficiency (Cox 1958; ReVelle and Whitaker 1997). In this approach, the total source energy is related to the acoustic energy through an efficiency factor (ε). The reported values for (ε) have varied between 0.01% to a few percent (cf., Golitsyn et al. 1978), but the most recent work by ReVelle and Whitaker (1997) suggests that the most reasonable values are from 0.1% to a few percent. In

particular, the total acoustic energy (W_{total}) is related to the total energy (E) by:

$$W_{total} = \int_0^{\tau} \frac{\Delta P(t)}{\rho C_s} dt = \varepsilon \left(\frac{E}{2\pi R^2} \right) \Delta \quad (2)$$

where ε is the assumed acoustic efficiency, Δ is the attenuation (which will be a function of the range in general), ΔP is the pressure as a function of time observed at the station due to the disturbance, ρ is the mass density of the atmosphere at the receiver (which we take to be 1.225 kg m^{-3}), τ is the duration of the correlated energy from the event, and R is the range to the source.

To evaluate Equation 2, we must first compute the integral of the pressure signal. We numerically approximate the true signal at IS26 by:

$$\sum S^2 \cong \sum (S + n)^2 - 3 \sum n^2 \quad (3)$$

where we have assumed that $\Sigma Sn \sim \Sigma n^2$ (where S is signal and n is noise). Using this approximation, we derive upper limits for the integral in Equation 2 and solve for E. Taking C_s = 340 m/s, R = 370 km, and ignoring attenuation by setting Δ = 1, we find that E = 0.13 − 0.013 kT (5.4 − 0.5 × 10^{11} J) for $0.001 < \varepsilon < 0.01$, respectively.

An additional theoretical approach described in ReVelle (1976) uses only the period and slant range to the fireball under the assumption that the fireball can be represented as a line-source and that the signal is still a weak shock at the receiver. This latter assumption may not be strictly valid at the range of the receiver (370 km) in terms of the definition used by ReVelle (1976), but the resulting value provides an approximate (upper limit) estimate of the blast energy in the linear (acoustic) regime. The energy-period-range relationship is given by:

$$E_s = \frac{\pi}{12} \rho \left[\frac{\tau}{1.579} \right]^4 \left(\frac{C_s}{VR} \right) \quad (4)$$

where E_s is the source energy (in Joules), ρ is the meteoroid density (in kg m^{-3}), τ is the period at maximum amplitude (in sec), C_s is the mean sound velocity in air between the source and receiver, V is the velocity of the meteoroid in km/s, and R is the range in meters.

Using ρ = 3590 kg m^{-3}, as determined from the recovered meteorites, τ_1 = 3.2 sec and τ_2 = 4.1 sec (with subscripts for trains 1 and 2 respectively), C_s = 310 m/s, V = 21000 m/s, and R = 3.7 × 10^5 m, which results in Es_1 = 0.13 kT = 5.4 × 10^{11} J and Es_2 = 0.36 kT = 1.5 × 10^{12} J.

For completeness sake, we will also estimate energies from equations developed strictly for ground-level. From low-altitude nuclear test data, Davidson and Whitaker (1992) determined a wind-corrected amplitude-yield relation of the form:

$$Y = 1.35 \times 10^{-7} A^{1.471} 10^{-0.02588 V_H} R^2 \quad (5)$$

where Y is the source yield in kT, A is the maximum peak-to-peak overpressure associated with the signal in microbars, V_H is the speed of the wind along a great circle path between the source and receiver at 50 km altitude in m/s, and R is the range from the source to the receiver in km.

Using our observed A = 0.233 Pa, with V_H = 2 m/s (as derived from the HWM wind model (Hedin et al. 1996) from the source-receiver at 50 km altitude) and R = 370 km, we deduce an upper limit of 0.06 kT = 2.5 × 10^{11} J for the energy of the fireball from this relation. This result should be viewed cautiously, however, as it is quite sensitive to changes in V_H (for such small absolute values), which is only approximately defined (but is expected to be largely neutral at this time of the year) through the HWM model.

A related method of estimating the original source yield can be found numerically by comparing the observed amplitude at the receiver with point source detonations of varying yields along the trajectory computed using the normal-mode prediction for a stationary spherical "point" source in the Pierce-Posey-Kinney model (Pierce and Posey 1970; Pierce and Kinney 1976). Here, we iterate the yields at each height to produce a model match to the observed amplitudes at the receiver. The resulting graph of yield versus height is shown in Fig. 1 over the height range of interest for the Morávka fireball. We note that this is physically similar to the empirical approach represented in Equation 5 except it is: a) theoretical; b) uses the true atmosphere appropriate to the event; and c) is scaled to the appropriate source height.

From Fig. 1, apparently, over the range of heights most probably responsible for the sound generation, an equivalent point energy of ~0.1 kT (4 × 10^{11} J) results. This result is relatively insensitive to the height chosen as the source for the event, so we believe it to be robust. We also note that it is within a factor of 2 of the wind-scaled amplitude result for empirical surface explosions found using Equation 5.

All source energy estimates using infrasound data are summarized in Table 1. They range from 0.01 to 0.6 kT (4 × 10^{10} to 2.5 × 10^{12} J). The preponderance of solutions, however, suggests a likely energy near 0.1 kT, equivalent to the meteoroid mass of ~1600 kg. Our current acoustic efficiency calculations have assumed that Δ = 1, which produces the maximum possible value, since other Δ values (>1) will reduce the efficiency due to propagation effects up- or down-wind from the source (see ReVelle and Whitaker [1997] for details). Our current results suggest a very low acoustic efficiency (~0.001) for the Morávka fireball event. We also note that the period at maximum amplitude solutions are larger than the mean value—an effect that has been noted in the past (ReVelle and Whitaker 1999). This typically happens because the semi-empirical AFTAC relationship was developed for much greater ranges and for much larger source energies.

Table 1. Estimates for the initial total energy for the Morávka fireball based on interpretation of the infrasound signal at IS26 using different techniques.

Acoustic technique	Energy estimate (kT)	Reference
Period at maximum amplitude	0.59 ± 0.28 (train 2)	ReVelle (1997)
Acoustic efficiency (ε = 0.001 – 0.01)	0.13 – 0.013	ReVelle and Whitaker (1997)
Weak-shock line source blast	0.13 (train 1); 0.36 (train 2)	ReVelle (1976)
Empirical ground-level explosion data	<0.06	Davidson and Whitaker (1992)
Numerical model yield stationary "point" source	0.1 ± 0.02	This study

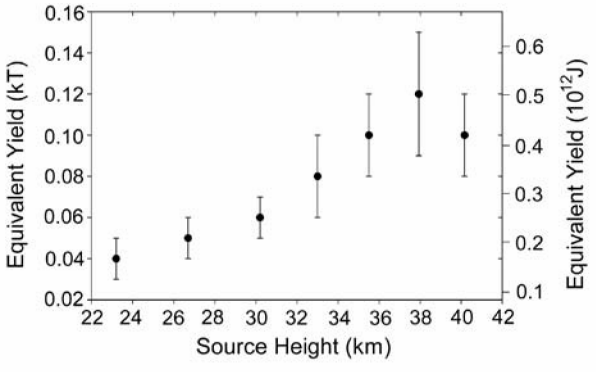

Fig. 1. Equivalent yield as a function of height along the trajectory of the Morávka fireball needed to produce the observed maximum peak-to-peak amplitude at IS26 (0.233 Pa).

Estimate from Noble Gases

Concentration and isotopic composition of He, Ne, and Ar, as well as the concentrations of the main isotopes of Kr and Xe have been determined in bulk samples of 2 meteorites, namely Morávka 1 and 2 (see Borovička et al. [2003] for the list of recovered meteorites). The techniques and methods were described recently by Scherer and Schultz (2000). The results of the measurements are given in Table 2.

Both meteorites show high shielding characterized by cosmogenic $^{22}Ne/^{21}Ne$ <1.09 (1.071 for meteorite 1, and 1.088 for meteorite 2). From the value of 1.07 for meteorite 1, we deduce a minimum meteoroid pre-atmospheric radius of 30 to 40 cm, similar to the recently analyzed St-Robert chondrite (Leya et al. 2001). We also tried to estimate the pre-atmospheric radius and the depth of the samples within the meteoroid from the combination of the $^{22}Ne/^{21}Ne$ ratio and the activity of cosmogenic ^{26}Al using the model of Graf et al. (1990). The ^{26}Al measurements for both Morávka 1 and 2 were taken from Neder et al. (2001). This approach yielded the radius of 90 ± 20 cm and depths of samples of about 12 to 40 cm. This radius and the corresponding meteoroid mass (5000–20000 kg), however, are much larger than estimates derived from the fireball radiation and infrasound production. A possible explanation of this discrepancy could be a 2-stage exposition history. ^{26}Al gives the production rate over the last few Ma, but the stable cosmogenic nuclides integrate over the whole time of irradiation. Taking the measured ^{26}Al activity and assuming the radius of 40 cm, the $^{22}Ne/^{21}Ne$ ratio should be about 1.14 from the model of Graf et al. (1990). However, if the material was irradiated earlier under high shielding, cosmogenic noble gases will build up with low $^{22}Ne/^{21}Ne$. After excavation, this ratio will change only slightly because of a much smaller exposure time.

Finally, we can look at the recent model calculation of Masarik et al. (2001). Although the cosmogenic Ne isotopes are still very difficult to calculate from basic principles, the model and $^{22}Ne/^{21}Ne$ measurements are both consistent with a meteoroid radius of 40–50 cm and a depth of about 15 cm for meteorite 2 and of 25–35 cm for meteorite 1.

In summary, if we ignore the ^{26}Al data, the $^{22}Ne/^{21}Ne$ ratio alone gives the most probable radius of 45 cm. If the ^{26}Al data are correct, either the model of Graf et al. (1990) is not applicable in this case or 2-stage exposure history is needed to explain the data.

Estimate from Seismic Data

Seismic signals from the Morávka fireball were recorded at 16 stations and are described in Brown et al. (2003). Air-coupled P-waves, air-coupled Rayleigh waves, and direct arrivals of airwaves were detected. The estimation of fireball energy from seismic data is difficult because of several uncertain factors. Very recently, Brown et al. (2002), in connection with the Tagish Lake fireball, proposed a formula relating the equivalent energy yield (W) (in kT TNT), the range to the source, (R) (in meters), and the average vertical ground motion of the Rayleigh waves (D_v) (in nm/s):

$$W = \chi\gamma^{-1}R^2(9.748\times10^{-11}D_v)^{1.738} \quad (6)$$

where χ is the ratio of the air-to-ground coupling efficiency for a surface explosion to airburst at altitude and γ is the attenuation factor of the Rayleigh wave amplitude due to the composition of the local ground relative to loose soil. Brown et al. (2002) used χ = 100 and γ = 0.1 for compact granitic rock.

We have at our disposal calibrated seismic signals from stations operated by DPB Paskov. Only station BMZ shows the Rayleigh waves clearly—the other stations are too close to the trajectory (see Brown et al. 2003). Nevertheless, we tried using the direct airwaves as well. They are transformed to the P-waves in the case of deep underground stations, and the efficiency factor might be similar to that of the Rayleigh

waves. For surface stations located close to the trajectory, where the incidence angle was near 90°, we used Equation 6 with $\chi = 1$. Taking into account that less compact rock than granite is present in the region, we used $\gamma = 0.2$. The measured wave amplitudes and resulting energy yields are given in Table 3. Following Brown et al. (2002), we computed the arithmetic mean of the amplitudes of the 3 largest cycles of the wave trains. The ranges are computed to the nearest point of the fireball trajectory. No obvious discrepancy exists between the results computed from direct airwaves and from Rayleigh waves. In either case, however, the resulting fireball energies vary by 2 orders of magnitude, which shows that no better than order-of-magnitude estimates can be expected from seismic data. Neglecting the outlying stations MAJ and CSM, the geometric mean from 6 remaining stations gives the value of 0.13 kT TNT.

We emphasize that Equation 6 is very crude and should be used with care. The efficiency factors certainly vary from site to site and for different types of waves and incidence angles and are poorly known for most specific stations. Methods other than seismic analysis are preferable for determining fireball total energy with precisions better than an order-of-magnitude.

Summary of Mass Estimates

Table 4 contains the overview of the estimates of the pre-atmospheric mass. Good agreement exists between the mass determinations from fireball luminosity and from the infrasonic data. The results from noble gases and seismic records are less certain but generally are consistent with radiation and infrasound data. We also incorporated the results obtained from radionuclides by Neder et al. (2001). They estimated the meteoroid radius to 25–30 cm and the depth of Morávka 2 to about 10–15 cm and of Morávka 1 to 25–30 cm, putting it near the meteoroid center (note that the depths of Morávka 1 and 2 were interchanged in the original paper by a misprint). The corresponding mass estimate of Neder et al. (2001) of about 300 kg is clearly too low because it would imply a fireball luminous efficiency of almost 50%. Again, a complex exposure history could be a possible explanation of the discrepancy. This hypothesis will be investigated in the future.

In principle, fireball dynamics in the atmosphere could also be used for a determination of meteoroid mass. However, the early fragmentation of the Morávka meteoroid discussed in Borovička and Kalenda (2003) made this impossible. Therefore, relying mainly on the radiation and infrasound data, we concluded that the pre-atmospheric mass of the Morávka meteoroid was 1500 ± 500 kg. This corresponds to an equivalent diameter slightly below 1 meter. The energy of the event was 0.09 ± 0.03 kT TNT. The integral luminous efficiency was 9 ± 4%, and the acoustic efficiency was 0.14 ± 0.06% or slightly more if the signal attenuation was significant.

METEOROID HISTORY

In this section, we will discuss the cosmic ray exposure age and other evidence from noble gases. In addition, the orbit of the meteoroid will be integrated backward to obtain qualitative information on the orbital history. The combination of both types of information will be discussed.

Cosmic Ray Exposure Age and Gas Retention Age

Cosmic ray exposure ages (CREA) were calculated from the cosmogenic nuclides ^{3}He, ^{21}Ne, and ^{38}Ar. At first, the procedures and production rates of Eugster (1988) were used. However, these corrected production rates are not valid for highly shielded samples characterized by cosmogenic ^{22}Ne/^{21}Ne <1.09. Therefore, we also used the production rates

Table 2. Noble gas concentrations (in 10^{-8} cm^3 STP/g) in two Morávka meteorites.[a]

Meteorite	Weight (mg)	^{3}He	^{4}He	^{20}Ne	^{21}Ne	^{22}Ne	^{36}Ar	^{38}Ar	^{40}Ar	^{84}Kr	^{132}Xe	^{129}Xe/^{132}Xe
1	109.0	5.23	388	1.88	2.04	2.19	1.30	0.50	3173	0.015	0.031	1.36
2	99.2	3.67	214	1.66	1.75	1.91	1.16	0.41	1243	0.013	0.024	1.40

[a]Uncertainties of individual measurements for He, Ne, and Ar are estimated to be <5%, and <10% for Kr and Xe. Larger variations are possibly due to sample inhomogeneities.

Table 3. Seismic wave amplitudes and inferred fireball energy yields.

Station	Waves	Range (km)	Amplitude (nm/s)	Energy (kT TNT)
BMZ	Rayleigh	38.3	867	0.37
MAJ[a]	DA →P	27.1	133	0.007
CSA[a]	DA →P	28.0	368	0.045
KVE[a]	DA →P	26.0	484	0.06
LUT	direct-air	29.8	11500	0.20
CSM	direct-air	25.9	27700	0.7
PRS	direct-air	30.5	11800	0.22
RAJ	direct-air	28.1	8090	0.10

[a]Deep underground station.

Table 4. The estimates of Morávka meteoroid pre-atmospheric mass, energy, and diameter from various types of data.

Data type	Mass (kg)	Energy (kT TNT = 4.185 × 10^{12} J)	Diameter (m)	Reference
Radiation	1400 (1000–2800)	0.08 (0.06–0.17)	0.90 (0.80–1.15)	This study
Infrasound	1600 (800–2500)	0.10 ± 0.05	0.95 (0.75–1.1)	This study
Noble gases	1400 (400–11000)	0.08 (0.025–0.7)	0.9 (0.6–1.8)	This study
Seismic	2100 (1000–5000)	0.13 (0.06–0.3)	1.05 (0.8–1.4)	This study
Radionuclides	300 (230–400)	0.02 ± 0.005	0.55 ± 0.05	Neder et al. (2001)
Accepted	1500 ± 500	0.09 ± 0.03	0.93 ± 0.12	

calculated according to the method of Graf et al. (1990) for a meteoroid of 90 cm radius and a shielding depth of 20 cm. This radius and depth were also derived from Graf et al.'s model (see the previous section), so the calculations should be mutually consistent. The results of both methods are given in Table 5. Using ^{21}Ne and ^{38}Ar only, mean values of CREA of 5.6 ± 0.9 Ma and of 7.3 ± 1.0 Ma were calculated by the methods of Eugster (1988) and Graf et al. (1990), respectively. Giving the latter method double weight, the overall average value is 6.7 ± 1.0 Ma. This falls within the well-known 7 Ma peak of H chondrites, which is also well-pronounced in the H5 chondrites alone (Marti and Graf 1992). CREAs calculated from ^{3}He are shorter than those calculated from ^{21}Ne or ^{38}Ar. This is indicative of a ^{3}He deficit, which is discussed below.

Gas retention ages were calculated from concentrations of the radiogenic isotopes ^{4}He and ^{40}Ar and mean concentrations of U and K in H chondrites (13 ppb and 780 ppm, respectively; Mason 1979). The cosmogenic component of ^{4}He is calculated using $(^{4}He/^{3}He)_c$ = 6.1 (Alexeev 1998) and ^{40}Ar is taken as completely of radiogenic origin. These results are compiled in Table 5. The retention age computed from ^{4}He is significantly lower than that computed from ^{40}Ar. This indicates a loss of ^{4}He similar to ^{3}He. Even the ^{40}Ar gas retention ages are relatively low in both meteorites, which shows that this material was involved in thermal events rather recently. Loss of radiogenic gas can take place on the parent body of the meteorite (e.g., during the impact that produced the meteoroid), but, considering the case of ^{3}He, the loss was possibly due to solar heating at small perihelion distances.

Helium Deficit

As shown above, both the cosmic ray exposure age computed from cosmogenic ^{3}He and the gas retention age computed from radiogenic ^{4}He are lower than the same ages computed from other gases. This is a demonstration of helium deficit in the meteorite. For ^{3}He, the deficit can also be seen in the so-called Bern plot where both Morávka samples fall below the field generally occupied by chondritic samples having the full complement of ^{3}He (Fig. 2). The deficit of ^{3}He in Morávka is at least 30%. Meteorites below the Bern line are traditionally assumed to have lost their cosmogenic ^{3}He by solar heating.

Recent calculations of Masarik et al. (2001) have shown that samples located inside large meteoroids (with radii above 60 cm) can exhibit smaller ^{3}He/^{21}Ne ratios without helium loss. The authors suggested that complex exposure histories may be responsible for low ^{3}He content in some meteorites. Their model, however, did not produce ^{3}He/^{21}Ne ratios less than about 3.5. Therefore, in the case of Morávka, the loss of ^{3}He must have really occurred.

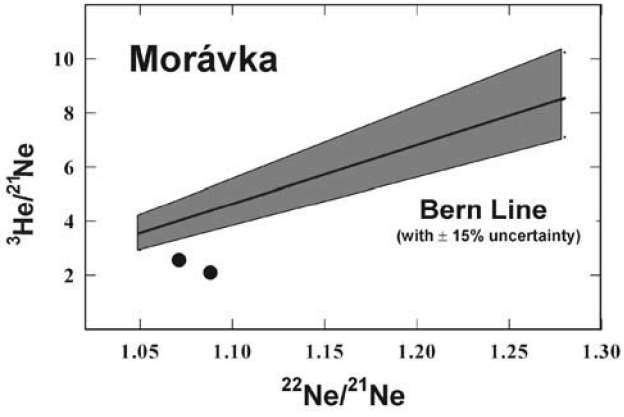

Fig. 2. Cosmogenic ^{3}He/^{21}Ne versus ^{22}Ne/^{21}Ne ratio in 2 Morávka meteorites and the empirical Bern line for chondrites without ^{3}He deficit.

Graf et al. (2001) have identified an anomalous group of H5 chondrites characterized by a high percentage of morning (a.m.) falls, exposure ages of 7.0 Ma, and a deficit of ^{3}He expressed in terms of the ^{3}He/^{38}Ar ratio in metal. Some characteristics of Morávka resemble this group. Morávka is also H5 chondrite with 7 Ma exposure age and it could well have fallen before noon because the meteoroid came from the north and it was only a matter of few 1000 km that determined the time zone in which the fall would occur. The deficit of ^{3}He in metal in the anomalous group was explained by the diffusion of its precursor ^{3}H under elevated temperatures. The members of the group are believed to have had orbital perihelia smaller than the majority of other chondrites over most of the last 7 Ma. The actual values of perihelion distances are not known. However, in contrast to Morávka, the members of the anomalous group exhibit no significant deficit of ^{3}He in bulk ^{3}He/^{21}Ne ratios. Therefore, Morávka seems to have suffered even larger temperatures since ^{3}He was also lost from the silicate phase.

Morávka is, in fact, the first meteorite with a clear ^{3}He deficit and known orbital elements. The elements do not support the idea of anomalous heating because the perihelion distance is as large as 0.98 AU (Borovička et al. 2003).

Table 5. Radiogenic ^{4}He and ^{40}Ar and calculated gas retention ages and cosmic ray exposure ages calculated with production rates according to Eugster (1988) and Graf et al. (1990) for a meteoroid of 90 cm radius and a sample depth of 20 cm.

	^4He_r	$^{40}Ar_r$	Gas retention age (Ga)		Cosmic ray exposure age (Ma)			
Meteorite	(10^{-8}cm^3 STP/g)		U, Th-^{4}He	K-^{40}Ar	^{3}He	^{21}Ne	^{38}Ar	Method[a]
Morávka 1	356	3173	1.1	3.5	3.5	5.1	6.4	E88
	–	–	–	–	5.0	7.8	8.2	G90
Morávka 2	192	1243	0.6	2.2	2.6	4.7	5.0	E88
	–	–	–	–	3.5	6.7	6.3	G90

[a]E88 = Eugster (1988); G90 = Graf et al. (1990).

However, the orbits of Earth-crossing meteoroids are unstable and develop rapidly on the scale of Ma. Therefore, we performed numerical integration of the orbit to see how the orbit probably evolved in the past.

Orbital History

The qualitative orbital evolution of the Morávka meteoroid was studied using the orbital elements derived in Borovička et al. (2003). We used an 18th-order Taylor-Stephenson variable-step size integrator (see e.g., Sitarski 1979; Dybczynski and Jopek 1986). The dynamical model was the Newtonian N-body problem including 9 planets (Earth and the moon were considered as a single body) with masses and the state vectors taken from the JPL DE 405 Ephemeris (Standish et al. 1997).

The long-term integration of Morávka was carried out spanning the time interval from t = 0 (the osculating epoch 2451670.994480 TDT) back to t = −6 Ma. This interval nearly covers the cosmic ray exposure time of Morávka. The integration cannot be seen as the reconstruction of the real evolution of the meteoroid, nevertheless, it provides qualitative information about the general pattern of its orbital behavior. Because of the highly chaotic nature of the orbit, 4 particles with slightly different initial coordinates were integrated together with Morávka. Their coordinates were obtained by superimposing to the Morávka data a random noise of $R \times 10^{-4}$ AU and $R \times 10^{-6}$ AU/day, where R was a random number distributed uniformly between 0 and 1. The comparison of results for different particles shows the possible range of orbital evolution.

Figures 3–5 illustrate the orbital evolution of the Morávka meteoroid and 2 selected artificial Morávka-like particles. In general, within the integrated time interval, the orbits show slow-track evolution sometimes alternated by fast-track patterns. The slow-track evolution is characterized by random changes in the semimajor axis due to close approaches to the inner planets, while the fast-track evolution means strong and rapid changes in eccentricity due to resonances (Froeschle et al. 1995). In all cases, the Morávka evolution was dominated by chance close encounters with Earth (mainly), Mars, Venus, and occasionally with Mercury. This behavior is similar to the evolution of the bright bolides described in section 3.1 of Jopek et al. (1995). Besides the slow track behavior, we also observed the fast track characteristics when, from time to time, the particles were close or even locked to the secular resonance ν_3, ν_4, ν_5 and evolved close to the Kozai resonance. During the 6 Ma, the orbits continued to be Earth-crossing or at least Earth-approaching. The perihelion distances varied between 0.1 AU and 1.2 AU.

Figure 3 shows the orbital evolution of the Morávka meteoroid. We can distinguish 2 phases of the evolution. The first phase lasted from −6 Ma to −3 Ma. During this time, the large secular changes of the eccentricity (up to 0.95) took place, due to libration of the critical angle $\tilde{\omega} - \tilde{\omega}_J$ overlapped by the alternate changes of the $\tilde{\omega} - \tilde{\omega}_E$. During the first 2 Ma the Kozai resonance significantly influenced the changes of (e), (q) and in particular, the inclination of the orbit. The Morávka meteoroid was never locked into this resonance, but for a long time, the circulation of the argument of the perihelion (the indicator of the Kozai resonance) was varying slowly in the vicinity of the values of 0° and 180°, resulting in large changes of the orbital inclination. The first phase was finished by a series of deep close encounters with planets at −3 to −2.6 Ma. The second part of the Morávka evolution belongs to the slow-track type. The eccentricity oscillates around the value 0.5. The oscillation period (in particular during the last 1 Ma) is close to the circulation period of the critical argument $\tilde{\omega} - \tilde{\omega}_J$.

During 6 Ma evolution of the Morávka-like particle #2, the eccentricity oscillated around 0.45 between the values of 0.3 and 0.6. The perihelion distance was never smaller than 0.8 AU (see Fig. 4). One can distinguish 3 different stages here. The first one ended after 1.2 Ma when a deep close encounter with Earth had occurred. The encounter resulted in the big change of the semi-major axis. Before this event, oscillation of the elements (e) and (q) correlates with the changes of the critical argument $\tilde{\omega} - \tilde{\omega}_M$, pointing to the influence of the secular resonance ν_4 between the particle and Mars. The second part of the orbital evolution begins with libration of the critical angle $\tilde{\omega} - \tilde{\omega}_J$ of the ν_5 resonance. After some alternation between circulation and libration, the circulation of the critical angle with a period similar to the period of the eccentricity modulations started at −2 Ma (the third stage).

The numerical dynamical evolution of particle #3 (Fig. 5) looks like the slow-track one. We see the typical random walk

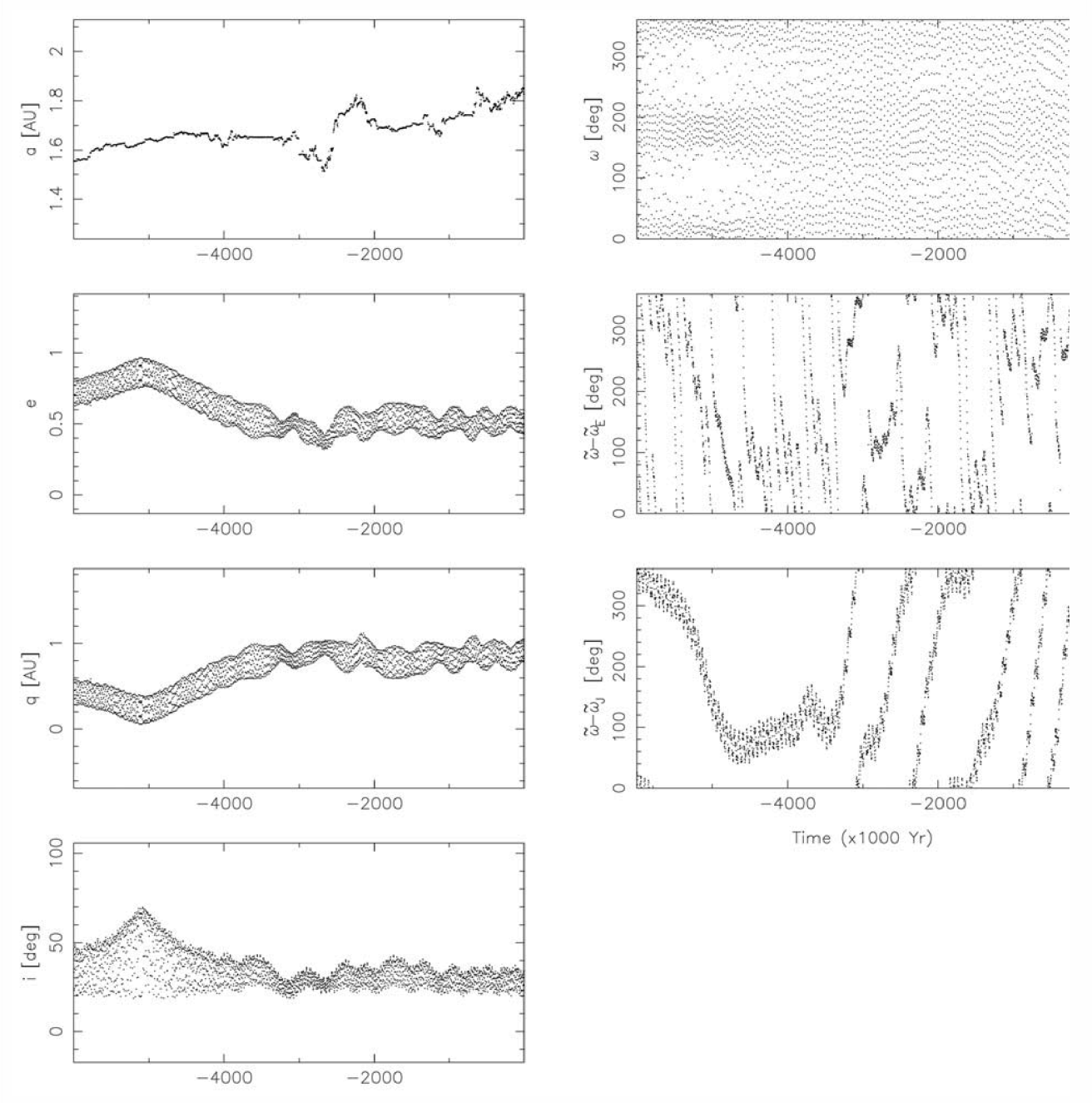

Fig. 3. Orbital evolution in the time span −6 Ma < t < 0 of the Morávka meteoroid. The figure shows the semimajor axis *a*, eccentricity (e), perihelion distance (q), inclination (I), argument of perihelion (w), and the critical arguments $\tilde{\omega} - \tilde{\omega}_E$ and $\tilde{\omega} - \tilde{\omega}_J$ of the ν_3 and ν_5 secular resonances.

pattern of the semi-major axis. The eccentricity and the perihelion distance change slowly and oscillate with the period correlated to the circulation period of the angle $\tilde{\omega} - \tilde{\omega}_J$. However, circulation is alternated regularly by the 0.2 Ma libration of this angle. The minimum perihelion distance is ~0.4 AU.

The presented examples of the numerical dynamical evolution of the Morávka-like particles are typical. However, the whole set of the possible orbital histories contains many different patterns, which points to a very chaotic nature of the movement. Nevertheless, at this stage of our studies, we think that a quasi slow-track pattern is typical for the evolution of the Morávka meteoroid. This also means that, at least during the last ~6 Ma, the Morávka meteoroid was orbiting on near-Earth-asteroid-type orbits. The inclination seems to be always larger than ~20°.

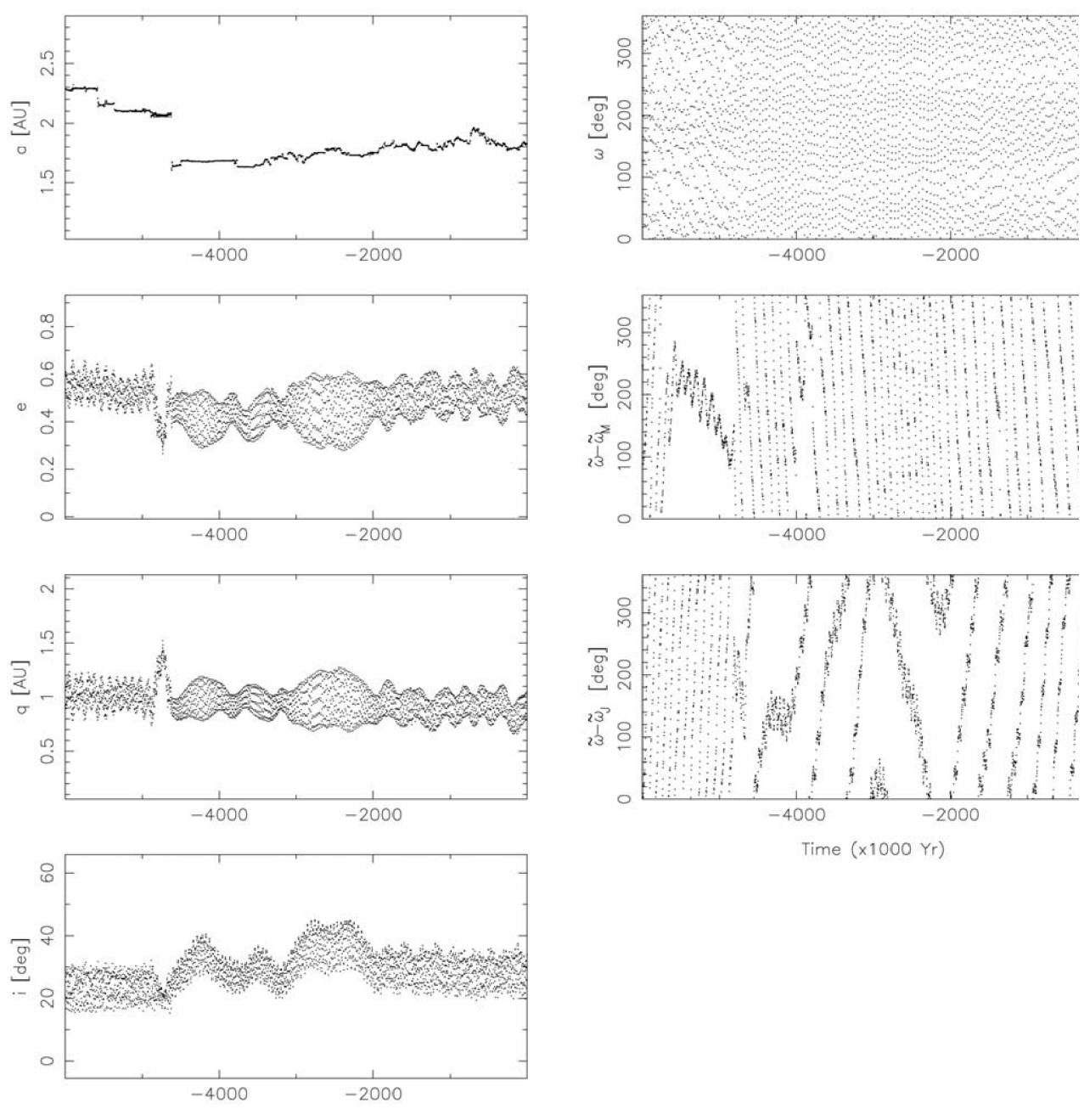

Fig. 4. Orbital evolution in the time span −6 Ma < t < 0 of the Morávka-like particle #2. The figure shows the semimajor axis (a), eccentricity (e), perihelion distance (q), inclination (I), argument of perihelion (w), and the critical arguments $\tilde{\omega}-\tilde{\omega}_M$ and $\tilde{\omega}-\tilde{\omega}_J$ of the ν_4 and ν_5 secular resonances.

Solar Heating

The orbital integration showed that the perihelion distance of the Morávka meteoroid probably reached quite low values during the ~6 Ma of its history as a separate body. The values of 0.4–0.5 AU are likely, and even perihelion distances as low as 0.1 AU may have been reached ~5 Ma ago. The temperature of the meteoroid at these distances from the sun can be estimated from a simple model. As a first approximation, the temperature (in K) is given by:

$$T = (\alpha/\varepsilon \cdot 0.25S/\sigma R^2)^{1/4} \quad (7)$$

where α is absorptivity; ε is emissivity; S is the solar constant;

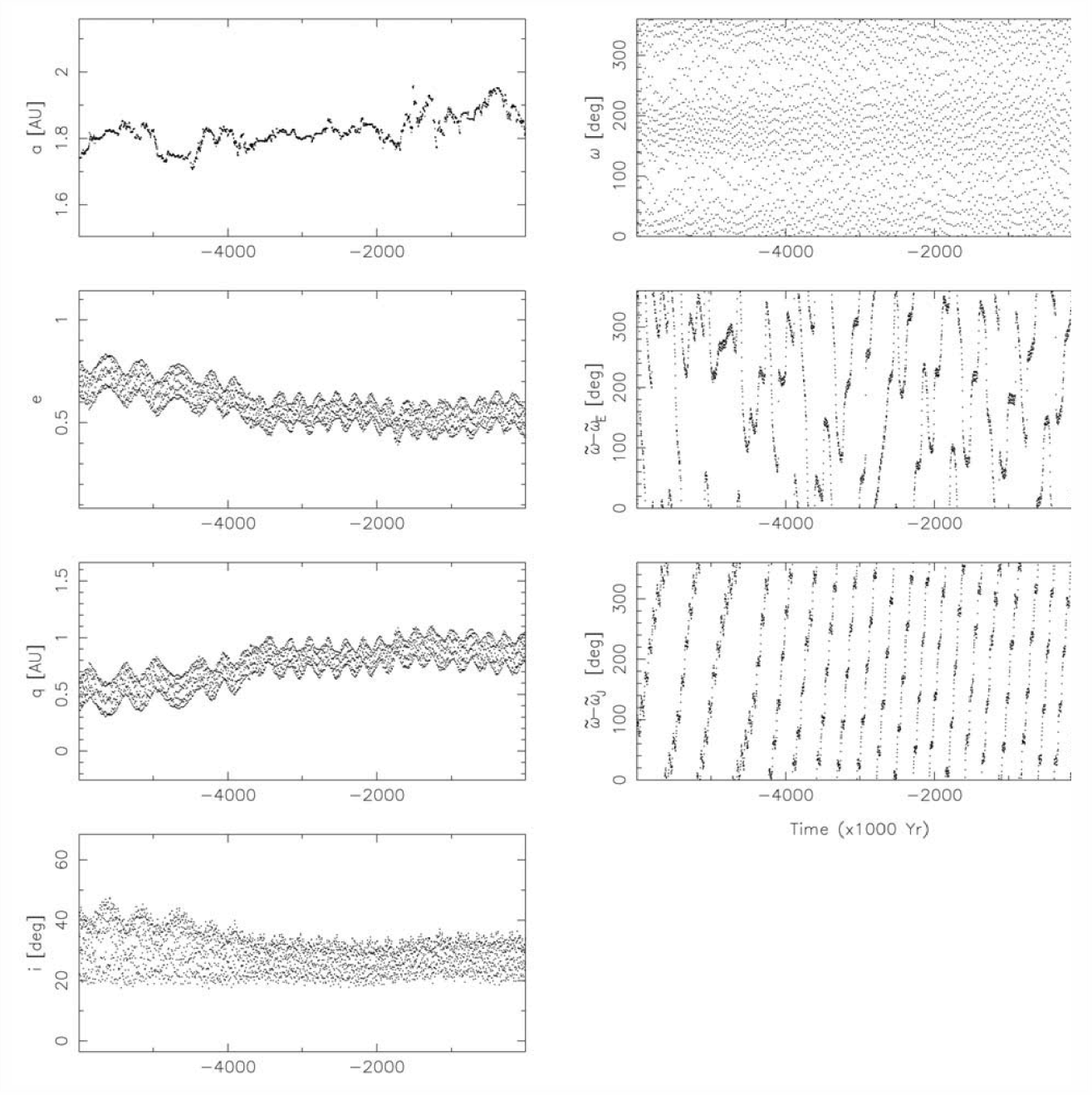

Fig. 5. Orbital evolution in the time span −6 Ma < t < 0 of the Morávka like particle #3. See the caption of Fig. 3 for explanation.

σ is the Boltzmann constant, and R is the distance from the sun in AU (Butler and Jenkins 1963). After substitution of the values of the constants, this becomes:

$$T = 278(\alpha/\varepsilon \cdot 1/R^2)^{1/4} \quad (8)$$

Using values of $\alpha = 0.65$ and $\varepsilon = 0.85$ suggested by Staley (1966), the equilibrium temperature of meteoroids as a function of distance from the sun is given in Fig. 6. For comparison, the line for $\alpha/\varepsilon = 1$ is drawn also. The meteoroid temperature at 0.5 AU is ~100°C or slightly higher. At 0.1 AU, the temperature reaches 500–600°C.

Huneke et al. (1969) computed ^{3}He and ^{21}Ne loss from meteoritic pyroxene and olivine at low temperatures. They conclude that ^{3}He and radiogenic ^{4}He are lost at temperatures of 100°C, or even less. Alexeev (2000), on the other hand, considers the temperatures of ~100°C much too low for significant diffusion losses of gases and takes the temperature of 400°C as appropriate for gas loss.

Comparing Morávka with another H5 chondrite with a

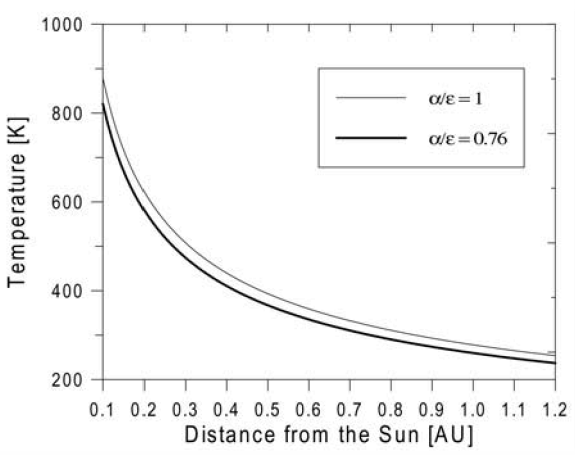

Fig. 6. The computed equilibrium temperature of a meteoroid as a function of distance from the sun. The dependence is given for 2 absorptivity to emissivity ratios.

known orbit, the Lost City (McCrosky et al. 1971), is interesting. The content of noble gases in this meteorite (Bogard et al. 1971) puts it near the Bern line. The orbital integration by Jopek et al. (1995) showed that the perihelion distance may have dropped to ~0.6 AU for a relatively brief period of time 1.3 Ma ago. Most of the time, however, the perihelion distance was significantly larger.

The investigations done so far do not provide a definitive answer on how small the perihelion distance must be for significant gas loss to be observed in meteorites. The Morávka meteorite certainly shows loss of cosmogenic ^{3}He as well as radiogenic ^{4}He. While the recent orbital elements with a perihelion distance of 0.98 AU do not suggest a possible loss of He, the calculation of previous perihelion distances imply that values below 0.5 AU and possibly as low as 0.1 AU were reached during the meteoroid lifetime. This is consistent with significant helium depletion in comparison with typical meteorites that never came so close to the sun.

Summary of Meteoroid History

Morávka is 1 of only 6 meteorites with well-known orbits. Although the chaotic nature of the Earth-crossing orbits prevents an unambiguous determination of meteoroid orbital history, the main characteristics of the orbital evolution can be estimated. At the same time, the cosmic ray exposure age of 6–7 Ma and a significant helium deficit were found from the meteorite analyses.

The delivery of meteorites from the asteroid main belt has been the subject of numerous investigations. The scenario of Morbidelli and Gladman (1998) assumes that a collision in the asteroid belt injects small meteoroids into the resonances (mainly 3:1 and ν_6), and the meteoroids then evolve on fast tracks to Earth-crossing orbits. Because this mechanism proved to be too fast in comparison with typical meteorite CRE ages, the authors speculated that some delay exists between the collision excavating the meteoroids from the parent body and their entry into the resonances. For Morávka, however, this scenario is not consistent with the available data. We have shown that slow-track orbital evolution is typical for Morávka, and the collision which excavated Morávka likely occurred while the parent body was on a near-Earth orbit. Of course, this does not mean that the collision occurred near Earth because the aphelion always lies in the asteroid belt.

The Morávka orbital history is more compatible with the scenario of Vokrouhlický and Farinella (2000). This scenario includes the Yarkovsky effect, i.e., a force arising from anisotropically emitted thermal radiation from meteoroids. Orbits evolve slowly under the influence of this effect unless the meteoroid enters a resonance. The authors found that a typical meteorite undergoes 2 to 5 collisional break-ups on the way from the asteroid belt to Earth. This is compatible with the last collision of Morávka having occurred on an evolved orbit. Since the CRE age of Morávka is close to CRE ages of a large number of H chondrites, this raises the possibility that a significant number of H chondrites were born during the same collision. If so, the further evolution of the Morávka orbit was not typical because the helium loss seen in Morávka is not observed in the majority of meteorites. The perihelion distance of Morávka was potentially small during some periods. The actual values are not known, but they could be as small as 0.1 AU. In any case, the perihelion evolved rapidly. We are not surprised that the final collision with Earth occurred when the perihelion was close to 1 AU because the collision probability is highest under these circumstances.

METEORITE COMPOSITION AND STRUCTURE

In this section, to complement the information on meteoroid size, history, and content of noble gases, we summarize the data on meteorite mineralogy and chemical composition. We also give some details of meteorite structure and mechanical properties, since they are related to the behavior of the meteoroid in the atmosphere, which were studied by Borovička and Kalenda (2003).

Macroscopic Properties and Petrology

The bulk density of meteorites 1–3 was determined by measuring the mass and the volume of whole specimens. The weighted average of the density is 3.59 ± 0.06 g/cm^3. This is higher than the average density of H chondrites at 3.44 g/cm^3 found by Wilkinson and Robinson (2000) but is within the 2.87–3.74 g/cm^3 range that they found.

The shapes of the meteorites are irregular. None of the 4 recovered pieces have a complete fusion crust cover. The crust coverage ranges from 60% to 90%. The thickness of the crust on different surfaces varies from very thin up to almost 1 mm. The crust is dark brown with parallel up to radially arranged streaks, forming a striated pattern on the surface. The variable thickness and incomplete coverage of the crust shows that the

atmospheric fragmentation of the meteoroid continued during the final stages of ablation and even after the ablation stopped. No evidence exists to suggest that the meteorite split and that the crust-free surfaces were formed at the time of impact.

The interior of the meteorite is fresh light gray and has slightly inhomogeneous (compared to brecciated meteorites) structure. Chondrules of around 1 mm in size are barely visible on the fresh surface. Macroscopic and microscopic observations do not reveal any brecciated texture common in ordinary chondrites. Only a small number of chondrules are visible in microscopic pictures, even using backscattered electrons. Chondrules form about 10% of the volume of the meteorite. There are 2 types of chondrules. Pyroxene chondrules with radial texture (Fig. 7) seem to be the most abundant. Chondrules formed by olivine with a Ca-rich pyroxene rim (reaction rim?, see Fig. 8) are usually well preserved, however. Minor remnants of olivine and low-Ca pyroxene chondrules were observed, though most of the olivine is recrystallized into individual weakly shocked grains. Opaque phases (metals and sulphides) form less than 30% of the volume of the Morávka meteorite, individual mineral grains (including the chondrules) form another 60% of the volume, and about 10 vol% is formed by fine-grained polycrystalline material. The porosity is very low.

A few irregular darker planes were observed on a freshly broken surface, showing a slightly darker gray color reminiscent of the tectonic microcracks and fracture planes in terrestrial rocks. These structures are visible to the naked eye and are difficult to find and observe under a microscope, either in parallel or crossed polarization. They are formed by discontinuous fine-grained polycrystalline matrix minerals without any preferred orientation. These apparent cracks were probably created by mechanical forces (such as those due to collisions of interplanetary bodies) of moderate intensity.

Morávka shows all the typical mineralogical features of H chondrites and was intensively recrystallized and homogenized. Therefore, it can be classified as type H5–6. Though the meteorite seems to be highly recrystallized, no traces of melt were observed. Very weak undulatory extinction of large olivine grains was observed, and no mosaic structures were found. Using the scheme of Stöffler et al. (1991), the Morávka meteorite is classified as having a shock level of S2.

Mineralogy

Major element analyses of mineral phases were carried out using the EDS as well as WDS electron microprobe analyses. At the Czech Geological Survey, analyses were carried out using the ED methods with 10 keV for silicates, and 20 keV for metals and sulphides (analyst J. Frýda). Similar conditions and analytical equipment were used at the Institute of Geochemistry, Mineralogy and Mineral Resources at the Faculty of Science, Charles University in Prague (analyst J. Haloda and P. Týcová). In the Naturhistorisches Museum in Vienna, the ARL SEMQ electron microprobe was used to analyze olivines and low-Ca pyroxenes (analyst F. Brandstätter). Since we have found excellent agreement among analytical data in the 3 laboratories (the same probe standards were used), the results were combined into averages and the data were treated as a single file. The full set of analytical data (around 500 analyses) is available on CD-ROM upon request from the authors (P. Jakeš).

The representative analyses of individual mineral phases are given in Tables 6–13. The minerals can be briefly described as follows:

Olivine

Individual grains of olivine and the olivine in chondrules form a substantial part of the meteorite. The composition of olivine varies from Fa 17.9 to Fa 19.5 with an average value of Fa 18.8 (n = 26). Zoning of individual olivine grains was

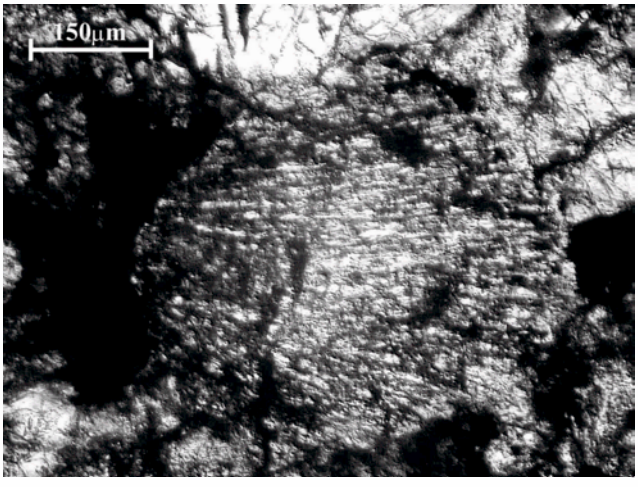

Fig. 7. Radial low-Ca pyroxene chondrule in the Morávka meteorite. Note the large recrystallized olivines in the upper right-hand corner. Crossed polarization.

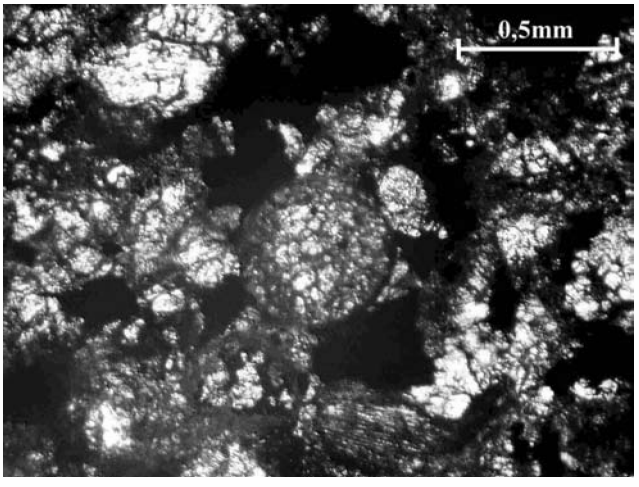

Fig. 8. Olivine chondrule with high-Ca pyroxene rim in the Morávka meteorite. Crossed polarization.

not observed. The content of minor elements Al, Ti, and Cr is very low and corresponds to the content of these elements in other ordinary chondrites.

Low-Ca Pyroxenes

The composition of low-Ca pyroxenes ranges from Fs 15.9 to Fs 17.2 (n = 28) with an average value of Fs 16.6. Compared to other ordinary chondrites, the calcium content is very low and Wo values of low-Ca pyroxenes vary between Wo 0.8 to Wo 1.3 (average is Wo 1.0). Generally, the Wo content is low. The Fa content of olivine matches the Fs content of low-Ca pyroxene for the H type chondrites. The plot of data from Morávka agrees well with other H chondrites (see, e.g., Fig. 181 of Brearley and Jones [1998]).

High-Ca Pyroxenes

High-Ca pyroxenes occur associated with plagioclases as well as with olivines. A zone of cpx with plagioclase rimming large olivine concentrations (chondrules) seems to exist. The composition of high-Ca pyroxene corresponds to Fs 6.4 and Wo 45.3. The average content of Cr (Cr_2O_3 = 0.95 wt%) is above the average for H5 or H6 chondrites. Two-pyroxene thermometry yielded the equilibration temperatures of about 800°C for the high-Ca pyroxene and 500–600°C for the low-Ca pyroxene.

Plagioclase

Plagioclase is a rare mineral the occurrance of which is usually associated with the high-Ca pyroxene either in the rims of the chondrules or in the "recrystallized" matrix. The composition varies over a relatively narrow range, although it seems that 2 types of plagioclase are present (plagioclase clearly associated with cpx ranges in Ab 76.5–87.5 and An 9.9–13.0, while plagioclase in recrystallized matrix appears less anothitic with An 2.6–7.5).

Phosphates

Phosphates analyzed in the Morávka meteorite are relatively Ca poor, being of merrillite type. The contents of FeO, Na_2O, and MgO correspond to composition of phosphates in the other ordinary chondrites of type 4–6. Though the volumetric amount of phosphate phase has not been measured, the rare earth element pattern indicates their higher than usual presence in Morávka (see below).

Chromites

Chromites analyzed in the Morávka meteorite show uniquely homogeneous composition, though slightly different from compositions in other H5–6 chondrites. The content of chromium oxide is higher and of FeO lower than in typical H6 chondrites.

Sulphides

Both troilite and pentlandite-rich sulphide components were encountered and analyzed.

Table 6. Representative analyses of olivines in the Morávka meteorite.

SiO_2	39.08	39.18	39.06	38.87	38.45
TiO_2	n.d.	n.d	0.07	0.02	n.d.
Al_2O_3	n.d.	0.02	n.d.	n.d.	n.d.
FeO	17.08	17.8	18.24	17.28	17.58
MnO	0.44	0.54	0.42	0.44	0.46
MgO	42.23	42.58	42.17	42.96	42.05
NiO	n.d.	0.13	0.2	0.15	n.d.
Cr_2O_3	n.d.	n.d	0.14	0.17	0.2
Sum	98.83	100.3	100.3	99.89	98.74

Table 7. Representative analyses of low-Ca pyroxenes in the Morávka meteorite.

SiO_2	56.07	57.49	57.12	55.76	56.22
TiO_2	0.04	n.d.	n.d.	0.20	0.21
Al_2O_3	0.74	0.45	0.07	n.d.	0.34
FeO	10.82	11.49	10.99	10.70	11.28
MnO	0.59	0.52	0.46	0.44	0.48
MgO	29.73	30.36	31.08	31.28	31.29
CaO	0.47	0.59	0.52	0.58	0.71
Cr_2O_3	0.19	0.34	0.05	0.13	0.17
NiO	0.03	n.d.	n.d.	n.d.	n.d.
Sum	98.68	101.24	101.24	100.29	99.09

Table 8. Representative analyses of high Ca-pyroxenes in the Morávka meteorite.

SiO_2	53.97	53.07	52.40	51.33	51.17	56.30
TiO_2	0.45	0.51	0.81	1.35	1.09	0.15
Al^2O^3	0.79	0.95	1.82	2.81	2.66	4.85
FeO	3.92	3.56	3.38	3.32	3.53	3.53
MnO	0.23	0.41	0.36	0.08	0.43	0.32
MgO	18.92	17.38	16.92	15.63	15.54	15.94
CaO	20.32	21.77	21.99	21.93	22.40	15.90
Na_2O	0.75	0.78	0.90	1.11	1.13	2.07
K_2O	n.d	n.d.	n.d.	0.02	n.d.	0.10
Cr_2O_3	0.82	1.56	1.43	1.99	2.12	0.44
Sum	100.18	99.98	100.02	99.58	100.06	99.61

Metals

Low nickel metal (kamacite) and high Ni metal (taenite) were analyzed in Morávka. The characteristic feature which separates Morávka from other H5–6 chondrites is relatively low nickel contents both in kamacite (around 4,5 wt%) as well as in taenite (47–50 wt% of Ni). The Si content is much lower in high Ni metals. Similarly, the Co content is higher in the low Ni phase (values up to 0,7 wt% of Co were measured).

CHEMICAL COMPOSITION

Instrumental neutron activation analysis, instrumental photon activation analysis, and radiochemical neutron activation analysis (INAA, IPAA, and RNAA, respectively) were employed for elemental characterization of the Morávka meteorite. Fractions of the ablation crust (mass of 13.10 mg containing approximately 55% of the "pure crust"), metallic,

Table 9. Representative analyses of plagioclases in the Morávka meteorite.

SiO_2	65.68	65.34	65.08	65.34
Al_2O_3	20.21	20.90	20.01	20.23
FeO	0.46	0.74	0.46	0.35
MnO	0.14	0.03	0.04	0.03
MgO	0.32	0.16	0.27	0.15
CaO	1.58	2.01	1.67	1.44
Na_2O	9.74	9.43	9.91	10.27
K_2O	0.67	0.74	0.69	0.56
Sum	98.81	99.36	98.12	98.38

Table 10. Analyses of phosphate phases in the Morávka meteorite.

Na_2O	2.56	2.64	2.60
MgO	3.34	3.38	3.23
P_2O_5	52.51	52.74	52.50
CaO	42.01	41.18	42.02
MnO	n.d	n.d	n.d
FeO	0.79	0.62	0.65
NiO	0.36	0.15	n.d
Sum	101.57	100.70	101.01

Table 11. Representative analyses of chromites in the Morávka meteorite.

MgO	2.32	2.32	2.40	2.58
Al_2O_3	6.03	5.98	6.08	5.74
SiO_2	0.37	0.40	0.47	0.33
TiO_2	1.78	1.92	1.82	2.33
Cr_2O_3	60.78	60.43	59.99	59.76
MnO	1.06	0.32	0.64	0.71
FeO	27.56	27.60	28.23	28.63
NiO	0.32	0.31	0.05	0.14
Sum	100.21	99.27	99.68	100.23

Table 12. Representative analyses of sulphides in the Morávka meteorite.[a]

	tr	tr	tr	tr	pen	pen
Si	0.25	0.24	0.11	0.07	0,07	0.18
S	35.68	36.68	36.47	36.48	33.81	33.09
Fe	63.40	63.17	63.12	62.65	50.07	50.31
Co	0.27	0.08	−0.04	0.03	−0.09	−0.04
Ni	−0.05	0.16	0.05	0.53	13.96	14.04

[a]tr = troilite; pen = pentlandite.

mainly iron grains (mass of 2.108 mg containing approximately 75% iron), and several aliquots of the meteorite bulk with masses in the range of 13.1 to 499.6 mg were taken for analysis. Irradiation for both short- and long-time INAA (1 min and 2 to 5 hr, respectively) was carried out in the LVR-15 experimental reactor of the Nuclear Research Institute Rez and placed at a thermal neutron fluency rate of 8×10^{13} cm^{-2} s^{-1} and a fast neutron fluency rate of 1.5×10^{13} cm^{-2} s^{-1}, while irradiation for IPAA was performed with bremsstrahlung produced with a 20 MeV microtron at the Institute of Raw Materials, Kutná Hora, operated at a 10 μA electron beam current. Gamma ray spectrometry measurement of the induced radionuclides was carried out using several high efficiency high-resolution HPGe detectors. The RNAA procedure employed for the determination of most of the rare earth elements (REE) was based on precipitation of their oxalates, while that for determination of Rb and Cs consisted in selective sorption of the elements on ammonium phosphomolybdenate. For quality control purposes, USGS rock reference materials (Basalt BCR-1 and Diabas W-1) were analyzed. Our results compared well with reference values, thus, proving the accuracy of the procedures employed. Details of the analysis and the results of control analyses are given in Randa et al. (2003).

In total, the abundances of 40 major, minor, and trace elements were determined by the above procedures. Some elements, namely Mg, Ca, Ti, Mn, Co, Ni, Sb, and Yb were assayed using 2–3 fully independent nuclear reactions, and the discovered results were in agreement. Thus, in addition to the routine quality control procedure, i.e., co-analysis of matrix-matched reference materials, another proof of accuracy was obtained employing the so-called self-verification principle of activation analysis (Byrne and Kucera 1996), which increases the credibility of the results achieved.

Table 14 shows the elemental composition of the 3 fractions of the meteorite analyzed. Rather scattered data were found for some elements, namely Fe, Co, and Ni. These variations are due to inhomogeneous distribution of metallic, mainly iron grains in the analyzed samples. The resulting bulk composition is compared in the last column with the average composition of H chondrites according to Wasson and Kallemeyn (1988). For the majority of elements, values within 20% of the average H chondrite composition were found. More deviating results still lay mostly within 3 standard deviations of the measurement errors. Only Br and Hg were highly enhanced (both 19 times the chondritic value), probably due to laboratory contamination, and were removed from Table 14. Significant enhancement by 35–50% was also found for Cs, La, and Ce. We do not have a clear explanation for this. Since these elements were determined in a single aliquot, though the heaviest of the meteorite, the presence of the phosphate phase and the unusual composition of the phosphate phase (described above) could account for the enrichment of the light rare earth elements La and Ce. The Cs (and also Rb) abundance in Morávka is much closer to CI chondrites than to H chondrites.

The ablation crust is enriched with siderophile elements Fe, Co, Ni, Ir, Au, as well as the volatile Sb, and is depleted in Si and Mg. The opposite result was obtained in the extended study of Genge and Grady (1999) who, however, concentrated on the outer crust. Since the metallic part is easier to melt and ablate than the silicate part, siderophile elements may, in fact, be underabundant in the outer crust and overabundant in the inner crust.

Table 13. Representative analyses of metal phases in the Morávka meteorite.

Si	0.08	0.01	0.16	0.19	0.13	0.19	0.16	0.12	0.05
S	0.01	0.04	0.07	–0.01	–0.04	0.10	0.03	0.04	0.05
Fe	90.79	93.47	93.30	94.90	94.92	52.00	51.90	50.56	52.82
Co	0.31	0.68	0.07	0.65	0.52	n.d.	n.d.	n.d.	0.30
Ni	6.92	5.76	5.88	4.78	4.66	47.21	46.76	49.51	47.21
Sum	98.11	99.97	99.48	100.51	100.19	99.13	98.67	100.23	100.42

Table 14. Elemental abundances in the Morávka meteorite.

Element, Unit	Method[a]	Ablation crust 13.10 mg	Metallic grains 2.108 mg	Bulk[b] 13–500 mg	Ratio to H chondrites
Na %	INAA	0.523 ± 0.016	0.115 ± 0.005	0.582 ± 0.038 (4)	0.91 ± 0.06
Mg %	INAA, IPAA	13.86 ± 0.42	2.99 ± 0.10	16.17 ± 0.81 (5)	1.16 ± 0.06
Al %	INAA	1.100 ± 0.033	0.253 ± 0.009	1.189 ± 0.089 (4)	1.05 ± 0.08
Si %	FINAA	12.7 ± 1.7	NA	18.1± 1.2 (1)	1.07 ± 0.07
Cl, μg g^{-1}	INAA	152 ± 16	157 ± 23	58 ± 22 (4)	0.7 ± 0.3
Ca %	INAA, IPAA	1.364 ± 0.050	0.168 ± 0.021	1.450 ± 0.116 (5)	1.16 ± 0.9
Sc, μg g^{-1}	INAA	7.98 ± 0.24	1.41 ± 0.08	8.56 ± 0.62 (2)	1.08 ± 0.8
Ti, μg g^{-1}	INAA, IPAA	550 ± 67	133 ± 32	770 ± 83 (1)	1.28 ± 0.14
V, μg g^{-1}	INAA	75.8 ± 2.4	41.3 ± 1.4	85.3 ± 5.1 (4)	1.15 ± 0.07
Cr, μg g^{-1}	INAA	3250 ± 100	1748 ± 54	3828 ± 154 (2)	1.05 ± 0.04
Mn, μg g^{-1}	INAA, IPAA	2288 ± 69	556 ± 17	2560 ± 188 (5)	1.10 ± 0.08
Fe %	INAA	30.68 ± 0.94	72.4 ± 2.2	24.03 ± 4.21 (3)	0.87 ± 0.15
Co, μg g^{-1}	INAA	1053 ± 32	3665 ± 110	575 ± 231 (6)	0.7 ± 0.3
Ni %	INAA, IPAA	2.20 ± 0.07	5.14 ± 0.18	1.38 ± 0.42 (7)	0.86 ± 0.26
Cu, μg g^{-1}	INAA	228 ± 19	141 ± 25	180 ± 52 (4)	2.2 ± 0.6
Zn, μg g^{-1}	INAA	45.4 ± 5.3	<100	43.2 ± 5.5 (2)	0.92 ± 0.12
As, μg g^{-1}	INAA	2.82 ± 0.26	9.7 ± 0.9	2.24 ± 0.42 (3)	1.1 ± 0.2
Se, μg g^{-1}	INAA	NA[c]	NA	7.7 ± 0.8 (1)	1.0 ± 0.1
Rb, μg g^{-1}	RNAA	NA	NA	2.26 ± 0.11 (1)	0.78 ± 0.04
Sr, μg g^{-1}	IPAA	NA	NA	12.0 ± 0.5 (1)	1.20 ± 0.05
Y, μg g^{-1}	IPAA	NA	NA	6.8 ± 2.3 (1)	3 ± 1
Zr, μg g^{-1}	IPAA	NA	NA	7 ± 3 (1)	1.1 ± 0.5
Sb, ng g^{-1}	INAA	740 ± 60	570 ± 120	110 ± 20 (1)	1.6 ± 0.3
Cs, ng g^{-1}	RNAA	NA	NA	177 ± 8 (1)	1.48 ± 0.07
La, ng g^{-1}	RNAA	NA	NA	440 ± 20 (1)	1.49 ± 0.07
Ce, ng g^{-1}	RNAA	NA	NA	1130 ± 60 (1)	1.36 ± 0.07
Pr, ng g^{-1}	RNAA	NA	NA	170 ± 20 (1)	1.38 ± 0.16
Nd, ng g^{-1}	RNAA	NA	NA	750 ± 90 (1)	1.19 ± 0.14
Sm, ng g^{-1}	RNAA	NA	NA	217 ± 9 (1)	1.17 ± 0.05
Eu, ng g^{-1}	RNAA	NA	NA	77.6 ± 3.7 (1)	1.06 ± 0.05
Gd, ng g^{-1}	RNAA	NA	NA	290 ± 40 (1)	0.97 ± 0.13
Tb, ng g^{-1}	RNAA	NA	NA	44 ± 3 (1)	0.83 ± 0.06
Ho, ng g^{-1}	RNAA	NA	NA	71 ± 3 (1)	0.97 ± 0.13
Tm, ng g^{-1}	RNAA	NA	NA	34 ± 5 (1)	0.87 ± 0.13
Yb, ng g^{-1}	RNAA	NA	NA	240 ± 14 (1)	1.17 ± 0.07
Lu, ng g^{-1}	RNAA	NA	NA	31.1± 1.5 (1)	1.00 ± 0.05
Ir, ng g^{-1}	INAA	960 ± 30	1780 ± 60	600 ± 200 (3)	0.79 ± 0.26
Au, ng g^{-1}	INAA	316 ± 10	1090 ± 60	236 ± 42 (4)	1.1 ± 0.2

[a]INAA = instrumental neutron activation analysis; FINAA = instrumental neutron activation analysis with fast neutrons; RNAA = radiochemical neutron activation analysis; IPAA = instrumental photon activation analysis.

[b]Mean uncertainty (inhomogeneity included) for N >1 (N = number of aliquots analyzed is given in parentheses). In other cases, the combined uncertainty of a single determination is given.

[c]NA = not applicable.

CONCLUSIONS

We used 4 independent methods (based on fireball radiation, production of infrasound, production of seismic signal, and content of cosmogenic isotopes in the meteorite) to determine the pre-atmospheric size of the Morávka meteoroid. Though the uncertainties of the individual methods are rather large, all methods gave consistent results.

The best estimate of the pre-atmospheric mass is (1500 ± 500) kg, corresponding to a diameter slightly less than 1 m and kinetic energy just below 0.1 kt TNT. Evaluation of fireball luminosity and evaluation of the infrasound using the numerical model yield approach proved to be the most promising methods for determining the meteoroid initial mass. The fireball integral bolometric luminous efficiency was found to be 9%, and the acoustic efficiency was about 0.14%.

From the point of view of meteoritics, the recovered meteorites are not exceptional. They are ordinary chondrites of common type H5–6. Nevertheless, several unusual aspects exist. Morávka is the first meteorite with a clear deficit of helium and a known orbit. The pre-atmospheric orbit, however, does not suggest any greater solar heating than is the case for other meteorites, since the perihelion distance was large (0.98 AU). The cosmic ray exposure age of the meteorite is 6.7 ± 1.0 Ma. The numerical integration of the orbit over this period showed that the orbit continued to be a near-Earth-type, and the collision that excavated Morávka likely occurred while the parent body was on a near-Earth orbit as opposed to an orbit in the main asteroid belt. The perihelion distance varied widely and probably decreased below 0.5 AU, and possibly even to 0.1 AU, about 5 Ma ago. This may help to explain the helium deficit.

The Morávka meteorites are also conspicuous in that none of the 6 recovered pieces was completely covered by a fusion crust. This is not usual. For example, 18 of 20 fragments of the St-Robert H5 fall had complete fusion crust coverage (Brown et al. 1996) and similar proportions were found among the dozens of fragments of the Mbale L5–6 meteorite shower (Jenniskens et al. 1994). Also, the majority of the Lost City and Príbram H5 chondrites had complete fusion crusts (McCrosky et al. 1971; Ceplecha 1961). So, while the atmospheric fragmentation of meteoroids is quite common, Morávka was more prone to repeated break-ups, continuing even after ablation ceased. The meteorite interior, however, does not show much difference from other ordinary chondrites. The Morávka meteorites are quite strong with low porosity and a bulk density higher than the chondritic average (3.59 g cm^{-3}) and have a low shock state (S2). The only hints of structural weakness are the apparent fine cracks seen by the naked eye but hardly visible in a microscope. These structural inhomogeneities were probably formed during collisions in interplanetary space, but how Morávka history differs from other meteorites in this respect and whether the once low perihelion distance played any role in forming or modifying the cracks is not clear. The Morávka meteorites also show minor deviations from other H chondrites in the abundances of some trace elements, namely La, Ce, Cs, and Rb.

Acknowledgments–We thank the meteorite finders J. Manoušek, J. Vlcek, and M. Vihnár who provided the meteorites for scientific research before the meteorites were actually purchased. P. A. Dybczynski helped us with the JPL DE 405 Ephemeris for orbital history calculation. The work of T. Jopek on orbital dynamics was supported by the KBN Project 2–P03–D–007–22. The work on meteorite mineralogy and petrology was partly supported by grant #313005 from the Ministry of Education of the Czech Republic.

Editorial Handling—Dr. Donald Brownlee

REFERENCES

Alexeev V. A. 1998. Parent bodies of L and H chondrites: Times of catastrophic events. *Meteoritics & Planetary Science* 33:145–152.

Alexeev V. A. 2000. Diffusion losses of inert gases in ordinary chondrites (abstract #1062). 31st Lunar and Planetary Science Conference.

Bogard D. D., Clark R. S., Keith J. E., and Reynolds M. A. 1971. Noble gases and radionuclides in Lost City and other recently fallen meteorites. *Journal of Geophysical Research* 76:4076–4083.

Borovička J. and Kalenda P. 2003. The Morávka meteorite fall. 4. Meteoroid dynamics and fragmentation in the atmosphere. *Meteoritics & Planetary Science*. This issue.

Borovička J. and Spurný P. 1996. Radiation study of two very bright terrestrial bolides and an application to the comet S-L 9 collision with Jupiter. *Icarus* 121:484–510.

Borovička J., Popova O. P., Nemtchinov I. V., Spurný P., and Ceplecha Z. 1998. Bolides produced by impacts of large meteoroids into the earth's atmosphere: Comparison of theory and observations. I. Benesov bolide dynamics and fragmentation. *Astronomy and Astrophysics* 334:713–728.

Borovička J., Spurný P., Kalenda P., and Tagliaferri E. 2003. The Morávka meteorite fall. 1. Description of the events and determination of the fireball trajectory and orbit from video records. *Meteoritics & Planetary Science.* This issue.

Brearley A. J. and Jones R. H. 1998. Chondritic meteorites. In *Planetary materials,* edited by Papike J. J. Washington D.C: Mineralogical Society of America. *Reviews In Mineralogy* 36:3-1–3-398.

Brown P., Hildebrand A. R., Green D. W. E., Page D., Jacobs C., ReVelle D., Tagliaferri E., Wacker J., and Wetmiller B. 1996. The fall of the St-Robert meteorite. *Meteoritics & Planetary Science* 31:502–517.

Brown P., ReVelle D. O., Tagliaferri E., and Hildebrand A. R. 2002. An entry model for the Tagish Lake fireball using seismic, satellite, and infrasound records. *Meteoritics & Planetary Science* 37: 661–676.

Brown P. G., Kalenda P., ReVelle D. O., and Borovička J. 2003. The Morávka meteorite fall. 2. Interpretation of infrasonic and seismic data. *Meteoritics & Planetary Science.* This issue.

Butler C. P. and Jenkins R. J. 1963. Temperature of an iron meteoroid in space. *Science* 142:1567–1568.

Byrne A. R. and Kucera J. 1997. Role of the self-validation principle of NAA in quality assurance of bioenvironmental studies and in the certification of reference materials. Proceedings, International Symposium on Harmonization of Health-Related Environmental Measurements Using Nuclear and Isotopic Techniques (Paper IAEA-SM-344/8). pp. 223–238.

Ceplecha Z. 1961. Multiple fall of Pribram meteorites photographed. 1. Double-station photographs of the fireball and their relations to the found meteorites. *Bulletin of the Astronomical Institutes of Czechoslovakia* 12:21–47.

Ceplecha Z., Borovička J., Elford W. G., ReVelle D. O., Hawkes R. L., Porubcan V., and Šimek M. 1998. Meteor phenomena and bodies. *Space Science Reviews* 84:327–471.

Cox E. G. 1958. Sound propagation in air. In *Handbuch der Physik.* Berlin: Springer Verlag. pp. 455–478.

Davidson M. and Whitaker R. W. 1992. *Miser's gold.* Los Alamos: Los Alamos National Laboratory. 28 p.

Dybczynski P. A. and Jopek T. J. 1986. ALPL-1 Newtonian ephemeris of the planetary system spanning 4000 Years. *Acta Astronomica* 36:153–164.

Eugster O. 1988. Cosmic ray production rates for ^{3}He, ^{21}Ne, ^{38}Ar, ^{83}Kr, and ^{126}Xe in chondrites based on ^{81}Kr/Kr exposure ages. *Geochimica et Cosmochimica Acta* 52:1649–1659.

Froeschle C., Hahn G., Gonczi R., and Farinella P. 1995. Secular resonances and the dynamics of Mars-crossing and near-Earth asteroids. *Icarus* 117:45–61.

Genge M. J. and Grady M. M. 1999. The fusion crust of stony meteorites: Implications for the atmospheric reprocessing of extraterestrial materials. *Meteoritics & Planetary Science* 34: 341–356.

Golitsyn G. S., Grigor'yev G. I., and Dokuchayev V. P. 1978. Generation of acoustic-gravity waves by meteor motion in the atmosphere. *Izvestiya Atmospheric and Oceanic Physics* 13:633–639.

Graf T., Baur H., and Signer P. 1990. A model for the production of cosmogenic nuclides in chondrites. *Geochimica et Cosmochimica Acta* 54:2521–2534.

Graf T., Caffee M. W., Marti K., Nishiizumi K., and Ponganis K. V. 2001. Dating collisional events: ^{36}Cl-^{36}Ar exposure ages of H chondritic metals. *Icarus* 150:181–188.

Hedin A. E., Fleming E. L., Manson A. H., Schmidlin F. J., Avery S. K., Clark R. R., Franke S. J., Fraser G. J., Tsuda T., Vial F., and Vincent R. A. 1996. Empirical wind model for the upper, middle, and lower atmosphere. *Journal of Atmospheric and Terrestrial Physics* 58:1421–1447.

Huneke J. C., Nyquist L. E., Funk H., Köppel V., and Signer P. 1969. The thermal release of rare gases from separated minerals of the Mocs meteorite. In *Meteorite research,* edited by Millman P. M. Dordrecht: Reidel. pp. 901–921.

Jenniskens P., Betlem H., Betlem J., Barifaijo E., Schluter T., Hampton C., Laubenstein M., Kunz J., and Heusser G. 1994. The Mbale meteorite shower. *Meteoritics* 29:246–254.

Jopek T. J., Farinella P., Froeschlé C., and Gonczi R. 1995. Long-term dynamical evolution of the brightest bolides. *Astronomy and Astrophysics* 302:290–300 (Erratum 314:353).

Leya I., Wieler R., Aggrey K., Herzog G. F., Schnabel C., Metzler K., Hildebrand A. R., Bouchard M., Jull A. J. T., Andrews H. R., Wang M. S., Ferko T. E., Lipschutz M. E., Wacker J. F., Neumann S., and Michel R. 2001. Exposure history of the St-Robert (H5) fall. *Meteoritics & Planetary Science* 36:1479–1494.

Marti K. and Graf T. 1992. Cosmic ray exposure history of ordinary chondrites. *Annual Review of Earth and Planetary Sciences* 20: 221–243.

Masarik J., Nishiizumi K., and Reedy R. C. 2001. Production rates of cosmogenic helium-3, neon-21, and neon-22 in ordinary chondrites and the lunar surface. *Meteoritics & Planetary Science* 36:643–650.

Mason B. 1979. Meteorites. In *Data of geochemistry,* edited by Fleischer M. Reston: U. S. Geological Survey. 132 p.

McCrosky R. E., Posen A., Schwartz G., and Shao C. Y. 1971. Lost City meteorite—Its recovery and a comparison with other fireballs. *Journal of Geophysical Research* 76:4090–4108.

Morbidelli A. and Gladman B. 1998. Orbital and temporal distributions of meteorites originating in the asteroid belt. *Meteoritics & Planetary Science* 33:999–1016.

Neder H., Laubenstein M., and Heusser G. 2001. Radionuclide concentrations in the freshly fallen meteorite Morávka (abstract). *Meteoritics & Planetary Science* 36:A146–A147.

Nemtchinov I. V., Svetsov V. V., Kosarev I. B., Golub' A. P., Popova O. P., Shuvalov V. V., Spalding R. E., Jacobs C., and Tagliaferri E. 1997. Assessment of kinetic energy of meteoroids detected by satellite-based light sensors. *Icarus* 130:259–274.

Pierce A. D. and Kinney W. A. 1976. *Computational techniques for the study of infrasound propagation in the atmosphere, Final report.* Washington D.C.: National Technical Information Service. 186 p.

Pierce A. D. and Posey J. W. 1970. *Theoretical prediction of acoustic-gravity pressure waveforms generated by large explosions in the atmosphere.* Bedform: Air Force Cambridge Research Laboratories.

Randa Z., Kucera J., and Soukal L. 2003. Elemental characterization of new Czech meteorite "Morávka" by neutron and photon activation analysis. *Journal of Radioanalytical and Nuclear Chemistry* 257:275–283.

ReVelle D. O. 1976. On meteor-generated infrasound. *Journal of Geophysical Research* 81:1217–1240.

ReVelle D. O. 1980. Interaction of large bodies with the Earth's atmosphere. In *Solid particles in the solar system,* edited by Halliday I. and McIntosh B. A. Dordrecht: Reidel. IAU Symposium 90. pp. 185–198.

ReVelle D. O. 1997. Historical detection of atmospheric impacts of large super-bolides using acoustic-gravity waves. *Annals of the New York Academy of Sciences* 822:284–302.

ReVelle D. O. and Ceplecha Z. 2002. Semi-empirical fragmentation model of meteoroid motion and radiation during atmospheric penetration. In *Asteroids, Comets, Meteors 2002,* edited by Warmbein B. ESA Special Publication #500. pp. 285–288.

ReVelle D. O. and Whitaker R. W. 1997. Acoustic efficiency analysis using infrasound from NEOs. In *Proceedings of the 5th International Conference on Space 96,* edited by Johnson S. W. Albuquerque: American Society of Civil Engineers.

ReVelle D. O. and Whitaker R. W. 1999. Infrasonic detection of a Leonid bolide: November 17, 1998. *Meteoritics & Planetary Science* 34:995–1005.

Scherer P. and Schultz L. 2000. Noble gas record, collisional history, and pairing of CV, CO, CK, and other carbonaceous chondrites. *Meteoritics & Planetary Science* 35:145–153.

Sitarski G. 1979. Recurrent power series integration of the equations of comet's motion. *Acta Astronomica* 29:401–411.

Staley D. O. 1966. Temperatures of meteoroids and meteorites. *Journal of Geophysical Research* 71:5681–5687.

Standish E. M., Newhall X. X., Williams J. G., and Folkner W. M. 1997. *JPL Planetary and Lunar Ephemeris.* Richmond: Willmann-Bell. CD-ROM.

Stöffler D., Keil K., and Scott E. R. D. 1991. Shock metamorphism of ordinary chondrites. *Geochimica et Cosmochimica Acta* 55: 3845–3867.

Vokrouhlický D. and Farinella P. 2000. Efficient delivery of meteorites to the earth from a wide range of asteroid parent bodies. *Nature* 407:606–608.

Wason J. T. and Kalleymen G. W. 1988. Composition of chondrites. *Philosophical Transactions of the Royal Society of London A* 325:535–544.

Wilkinson S. L. and Robinson M. S. 2000. Bulk density of ordinary chondrite meteorites and implications for asteroidal internal structure. *Meteoritics & Planetary Science* 35:1203–1213.